Face-centered-cubic K_3B_{80} and Mg_3B_{80} metals: Covalent and ionic bondings

Qing-Bo Yan, Qing-Rong Zheng, and Gang Su*
College of Physical Sciences, Graduate University of Chinese Academy of Sciences, P.O. Box 4588, Beijing 100049, China
(Received 28 October 2008; revised manuscript received 16 August 2009; published 23 September 2009)

By means of first-principles calculations within the density-functional theory, we find that stable face-centered-cubic (fcc) K_3B_{80} and Mg_3B_{80} solids can be formed. For both solids, two possibly stable geometrical phases (identified as phase *A* and phase *B*) with different lattice parameters can exist, where phase *A* has a lattice parameter smaller than phase *B*. In phase *A*, B_{80} clusters are significantly distorted and two or four intercluster covalent bonds are formed for K_3B_{80} or Mg_3B_{80}, respectively. In phase *B*, B_{80} units are slightly distorted and no intercluster covalent bonds exist. The phase *A* of Mg_3B_{80} bears the largest cohesive energy among them and is more stable than the fcc B_{80} solid. The charge population analysis shows that K and Mg are ionized and donate electrons to the other boron atoms of K_3B_{80} and Mg_3B_{80} solids. The different ionic radii of K and Mg lead to major geometrical differences between K_3B_{80} and Mg_3B_{80} solids and the competition of the covalent and ionic bondings could explain the emergence of two different geometrical phases for both. The electronic structural calculations reveal that both fcc K_3B_{80} and Mg_3B_{80} solids are metals.

DOI: 10.1103/PhysRevB.80.104111 PACS number(s): 81.05.Tp, 61.50.Ah, 71.20.Tx

I. INTRODUCTION

Boron is the fifth element and the neighbor of carbon in the periodic table. As is well known, carbon tends to form planar graphite, three-dimensional tetrahedral diamond, and spherical caged fullerenes[1,2] by sp^2 and sp^3 hybrid σ and π bonding. In contrast to the elegantly simple bonding manner of carbon, boron possesses a complicated bonding characteristic. Beside the normal σ bond, the so-called electron-deficient multicenter bonds[3] also play an important role in bonding resulting in richness and diversity in the structures of boron-related materials.[4] Nevertheless, many structural similarities present between carbon and boron, such as polycarbine-lithium boride, graphite-magnesium boride (MgB_2), and fullerenes-β-rhombohedral boron, are all conjugate analogies in structure.[5] Last year, another carbon analogy of boron, B_{80} buckyball, with a round and distinct hollow structure [Figs. 1(a) and 1(b)], has been predicted.[6] Such a boron fullerene, consisting of 80 boron atoms, is very similar in shape to C_{60} fullerene except that an additional boron atom sits in the center of each hexagon which significantly increases the stability of the cage.

After discovery of C_{60}, it has been unraveled that C_{60} clusters can condense to form solid phases such as the simple cubic (sc), face-centered-cubic (fcc),[7] and hexagonal-close-packed (hcp)[8] crystals. Furthermore, the alkali-metal-doped A_3C_{60} (A=alkali) fullerides based on the fcc C_{60} solid superconduct, with the transition temperatures ranging from 18 K (A=potassium) to 28 K (A=rubidium).[9] As B_{80} has a geometrical structure similar to C_{60} and boron and carbon could form similar structures as described above, it would be natural to anticipate that the boron fullerenes could also condense to form solid phases. In our previous work,[10] the boron buckyball B_{80} has been found that it could condense to form a stable fcc solid, in which the B_{80} units are geometrically distorted and four boron-boron chemical bonds are formed between every two nearest-neighbor B_{80} cages. In contrast to either the popular solid phases of pure boron that are usually insulating or semiconducting, or the sc, fcc, and hcp C_{60} solids that are band insulators,[11] the fcc B_{80} solid has a metallic electronic structure. The body-centered-cubic (bcc) B_{80} and K_6B_{80} solids have also been studied.[12] In this paper, we shall investigate the metal-doped K_3B_{80} and Mg_3B_{80} fcc solids by means of the first-principles density-functional theory (DFT) (Ref. 13) calculations. It is found that for both K_3B_{80} and Mg_3B_{80}, two different geometrical phases (identified as phase *A* and phase *B*) can be formed with different lattice parameters. In phase *A*, the B_{80} units are significantly distorted [Fig. 1(c)] and covalent bonds between the neighboring B_{80} units are formed resulting in geometries similar to the fcc B_{80} solid;[10] while in phase *B*, the B_{80} units are less distorted [Fig. 1(d)] and no bonds between B_{80} units are formed. The lattice parameters of both phase *A* and phase *B* of Mg_3B_{80} are about 0.3 Å smaller than that of K_3B_{80}; for both K_3B_{80} and Mg_3B_{80}, the lattice parameters of phase *A*

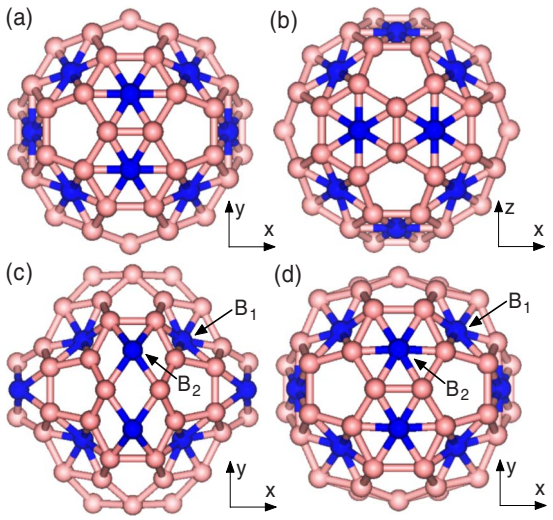

FIG. 1. (Color online) (a) Top view and (b) side view for an isolated B_{80} cluster. The distorted structures of B_{80} unit in the phase *A* (c) and phase *B* (d) of fcc K_3B_{80}, respectively. The blue (dark) balls denote the additional boron atoms at the center of hexagons, where two inequivalent types are labeled by B_1 and B_2.

are about 0.7 Å smaller than the phase *B*. The different ionic radii of K and Mg may bring major geometrical differences between K_3B_{80} and Mg_3B_{80} solids. The charge population analysis reveals that in K_3B_{80} or Mg_3B_{80}, each K or Mg atom donates about one electron to the other parts of the solid showing that ionic bondings exist in the solids. The competition of the covalent and ionic bondings may explain the emergence of two different geometrical phases. Similar to K_3C_{60}, the calculated electronic structures show that K_3B_{80} and Mg_3B_{80} solids are all metals.

II. COMPUTATIONAL DETAILS

All the calculations in this work are performed using the PWSCF code contained in the QUANTUM-ESPRESSO package.[14] This package is coded within the DFT framework based on pseudopotentials and plane-wave basis set. The interaction between electrons and ionic cores is imitated by Hamann-Schluter-Chiang norm conserving pseudopotentials[15] and the Perdew-Zunger[16] exchange-correlation potential within local-density approximation (LDA) (Ref. 17) is used. The kinetic energy cutoff of the plane-wave basis is taken as 30 Ry and the tolerance for absolute differences of the total energy is set as 5×10^{-5} Ry. The convergence of the total energy to the kinetic energy cutoff has been checked. The Brillouin zone is sampled on a uniform mesh of $4\times4\times4$ *k* points. To investigate the effects of different exchange and correlation, we recalculated the optimized geometries of K_3B_{80} and Mg_3B_{80} solid phases using the generalized gradient approximation. The optimized structures are nearly the same as the LDA results, while the cohesive energies are smaller than the corresponding values from LDA calculations. Such minor differences do not change the main conclusion. The situation is consistent with the results in Ref. 12.

The structures of fcc K_3B_{80} and Mg_3B_{80} solids have been set up by imitating the fcc K_3C_{60}, which has two tetrahedral and one octahedral interstitial sites per C_{60}.[18] The B_{80} clusters are put on the sites of fcc lattice, with the K or Mg atoms incorporated into the octahedral and tetrahedral interstices of the host lattice. Similar to the situation of fcc K_3C_{60},[19] there are only two possible orientations of B_{80} cluster that provide the most sufficient space for all intercalated K or Mg atoms. In both cases the B_{80} is oriented with eight of its 20 hexagonal faces along the cubic [111] directions. The two orientations are related by a 90° rotation about [100] direction. In the calculations, the *xy* plane of B_{80} clusters is arranged to be along the (100) plane of the fcc lattice as the starting configuration; i.e., the cubic crystallographic axes are aligned with the Cartesian axes.[20]

III. GEOMETRIES OF K_3B_{80} AND Mg_3B_{80} SOLIDS

In order to examine the stability of fcc K_3B_{80} and Mg_3B_{80} solids and to find the most favorable geometrical structures, for a series of fixed lattice parameters (denoted by *a* hereafter), we relax the atomic positions by the Broyden-Fletcher-Goldfarb-Shanno (BFGS) minimization[21] with a convergence tolerance of 5×10^{-4} Ry/bohr. For more clarity, the geometrical structures for every 0.1 Å between $a=13$ Å and $a=15$ Å, and every 1 Å between $a=15$ Å and $a=20$ Å are calculated, and the corresponding total energies are obtained. For the convenience to compare the stability of K_3B_{80} and Mg_3B_{80}, the cohesive energies (E_c) for every lattice parameter are then obtained according to the equation $E_c=E_{B_{80}}+3E_M-E_{M_3B_{80}}$, as visualized in Fig. 2. In the above equation, $E_{B_{80}}$ represents the total energy of an isolated B_{80}, which is simulated by a B_{80} cluster in a cubic supercell with a lattice parameter of 20 Å, and E_M represents the total energy of an isolated *M* (*M*=K,Mg) atom. As can be seen in Fig. 2, for both K_3B_{80} and Mg_3B_{80}, there are two minimums indicated by *A* and *B*, showing that both K_3B_{80} and Mg_3B_{80} have two possibly stable fcc solid phases, which we define as phase *A* and phase *B*, respectively. To check the stabilities of the above-obtained phase *A* and phase *B* of K_3B_{80} and Mg_3B_{80} further, full relaxations including the atomic positions, cell shape and volume are conducted by means of the BFGS minimization until the forces acting on atoms are less than a tolerance of 5×10^{-4} Ry/bohr. The results indicate that the geometries vary little showing that the obtained phase *A* and phase *B* of K_3B_{80} and Mg_3B_{80} are indeed stable. The lattice parameters and cohesive energies are listed in Table I. Interestingly, the lattice parameters of both phase *A* and phase *B* of Mg_3B_{80} are about 0.3 Å smaller than that of K_3B_{80}; for both K_3B_{80} and Mg_3B_{80}, the lattice parameters of phase *A* are about 0.7 Å less than phase *B*. The cohesive energies of both phase *A* and phase *B* of K_3B_{80} are about 16 eV/unit and

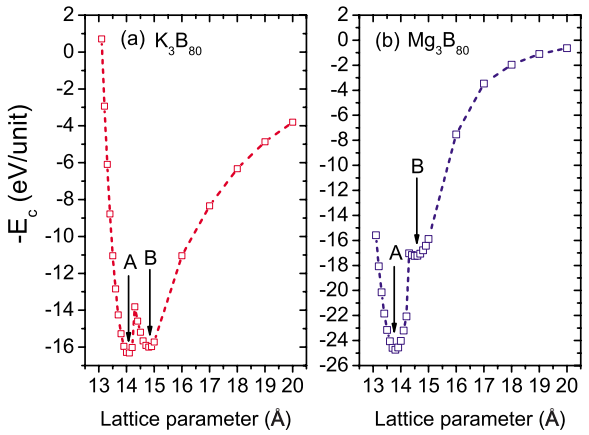

FIG. 2. (Color online) The cohesive energies (E_c) per K_3B_{80} and Mg_3B_{80} unit as functions of the lattice parameter. Letters *A* and *B* mark the corresponding lattice parameters and cohesive energies of phase *A* and phase *B* for both K_3B_{80} and Mg_3B_{80} solids.

TABLE I. The lattice parameters and cohesive energies (E_c) of different phases of K_3B_{80} and Mg_3B_{80} fcc solids.

	Phase	Lattice parameter (Å)	E_c (eV/unit)
K_3B_{80}	*A*	14.1	16.32
	B	14.8	16.00
Mg_3B_{80}	*A*	13.8	24.73
	B	14.5	17.24

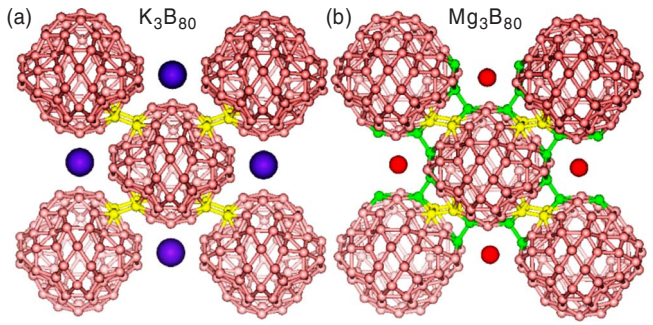

FIG. 3. (Color online) Schematic map of the bonding of the neighboring five B_{80} clusters in the (100) face of phase *A* fcc K_3B_{80} and Mg_3B_{80}. The purple and red balls indicate K and Mg atoms at the octahedral sites, respectively. Note that the K or Mg atoms at the tetrahedral sites are not shown here. The length of the yellow (gray) bonds between neighboring B_{80} units in (a) is 1.823 Å and the lengths of the yellow (gray) and green (dark) intercluster bonds in (b) are 1.730 and 1.783 Å.

that of phase *B* of Mg_3B_{80} is about 17 eV/unit. However, the phase *A* of Mg_3B_{80} has a much larger cohesive energy (about 25 eV/unit) and would be the most stable phase among them. It is also more stable than fcc B_{80},[22] whose cohesive energy is about 18 eV/unit (Ref. 10) showing that the Mg doping enhances the stability of the solid.

Recall that B_{80} units are geometrically distorted when they constitute fcc B_{80} solid. We checked the structural deformation of fcc K_3B_{80} as lattice parameters vary. When *a* is larger than 17 Å, B_{80} unit varies little and keeps the same spherical shape with the isolated B_{80}. As the lattice constant *a* decreases from 16 to 14.3 Å, the central atoms of the hexagons along the [111] direction (indicated by B_1 in Fig. 1) move inward gradually. The phase *B* of K_3B_{80} is at $a=14.8$ Å and the structure is shown in Fig. 1(d). In this phase, no chemical bond is formed between neighboring B_{80} units. As *a* proceeds to decrease, especially when *a* is between 14.3 and 14.2 Å, significantly geometrical distortions happen, which corresponds to the middle peak in Fig. 2(a), showing that a geometrical phase transition may occur. This transition leads to the emergence of the phase *A* of K_3B_{80}, which is at $a=14.1$ Å, with the structure of B_{80} unit very similar to that in fcc B_{80} solid,[10] as shown in Fig. 1(c). The central boron atoms of hexagons along the *z* axis (indicated by B_2 in Fig. 1) move outward and the sharing bonds are elongated and broken leading to a planar rhombus structure. In addition, B_1 atoms move inward remarkably enabling that B_{80} unit does not bear a spherical shape anymore. The transition also brings two covalent bonds formed between every two nearest-neighbor B_{80} units as shown in Fig. 3(a). It is worthy to note that the number of intercluster bonds is only half of that in fcc B_{80} solid and the bond length is also larger than that in fcc B_{80} solid suggesting that the K doping hinders the formation of intercluster bonds.

The geometrical evolution of fcc Mg_3B_{80} with the lattice parameter is similar to K_3B_{80}. When *a* varies from 20 to 14.5 Å, the structure of B_{80} unit is gradually changing, with B_1 atoms moving inward and no chemical bond is formed between B_{80} units. The phase *B* of Mg_3B_{80} is at 14.5 Å, with structure similar to that of K_3B_{80} [Fig. 1(d)]. The geometrical phase transition turns up at between 14.4 and 14.3 Å corresponding to the middle peak in Fig. 2(b). The phase *A* of Mg_3B_{80} is at 13.8 Å, with its B_{80} units structurally similar to that of K_3B_{80} [Fig. 1(c)]. However, in contrast to K_3B_{80}, four covalent bonds are formed between every two nearest-neighboring B_{80} units in phase *A* of Mg_3B_{80} and the bond lengths are 1.730 and 1.783 Å, smaller than that of K_3B_{80}, as demonstrated in Fig. 3(b). Thus, the covalent bonding in phase *A* of Mg_3B_{80} is stronger than that in K_3B_{80}, which may explain why the phase *A* of Mg_3B_{80} has a larger cohesive energy than phase *A* of K_3B_{80}. In both of phase *A* and phase *B* of Mg_3B_{80} and K_3B_{80}, although the B_{80} units are geometrically distorted, the symmetry of them remain T_h, i.e., the symmetry of isolated B_{80}.[23]

IV. BONDING AND ELECTRONIC STRUCTURES OF K_3B_{80} AND Mg_3B_{80} SOLIDS

The Löwdin charge populations are analyzed for the phase *A* and phase *B* of K_3B_{80} and Mg_3B_{80}. Here we focus on the valence charges of the boron atoms at centers of hexagons (B_1 and B_2), and K, Mg atoms, which are listed in Table II. In Table II, M_1 represents the K/Mg atoms at the octahedral sites, which are next to B_2 atoms, while M_2 denotes the K/Mg atoms at the tetrahedral sites, which are located between the hexagons along [111] directions and faces the B_1 atoms. Generally, for the phase *A* and phase *B* of K_3B_{80} and Mg_3B_{80}, B_1 and B_2 atoms lose a little charge (less than 0.2 electron), similar to the situation in the isolated B_{80} cluster,[24] where charges are transferred from the boron atoms at center of hexagons to the other boron atoms.[24,25] Meanwhile, both K and Mg atoms donate about one electron implying that K

TABLE II. The Löwdin valence charges of B, K, and Mg atoms in K_3B_{80} and Mg_3B_{80} fcc solids. B_1 and B_2 indicate two inequivalent types of boron atoms as in Fig. 1. M_1 and M_2 denote the K or Mg atoms at octahedral and tetrahedral sites, respectively.

		Löwdin charges			
	Phase	B_1	B_2	M_1	M_2
K_3B_{80}	*A*	2.9441	2.8871	0.0895	0.1186
	B	2.8417	2.8339	0.0911	0.1055
Mg_3B_{80}	*A*	3.0706	2.8939	0.9027	0.9412
	B	2.9967	2.8466	1.0196	1.5856

and Mg are ionized and ionic bondings exist in K_3B_{80} and Mg_3B_{80} solids. Note that in bcc K_6B_{80},[12] MgB_2 and CaB_6,[26] boron atoms also receive extra charges from K, Mg, and Ca atoms, respectively. Thus, it may be a general trend that the charges transfer from metallic atoms to boron atoms in boron-metal compounds.

Considering the fact that covalent, ionic, and van der Waals bondings may all exist in K_3B_{80} and Mg_3B_{80} fcc solids, we check again the geometries and energies of them and attempt to draw a picture to explain the geometrical phase transition and the emergence of the two geometrical phases. Take Mg_3B_{80} as an example. When a is larger than 17 Å, the gently sloping energy curve [see Fig. 2(b)] shows that the interactions between neighboring B_{80} units are weak, which could not cause changes in the shape of B_{80} clusters. As the nearest distance between the neighboring B_{80} units is greater than 3.85 Å, the van der Waals force may be the dominant interaction. When a is between 17 and 14.4 Å, the ionic bonding may become the major interactions, as the energy curve is sharp and the corresponding cohesive energy is large. The minimum B at $a=14.5$ Å is the equilibrium point of the ionic interaction and corresponds to the phase B of Mg_3B_{80}. When a further decreases, the distance between neighboring B_{80} units becomes small enough to form strong intercluster covalent bonds, leading to the structure of B_{80} unit distorted significantly to form bonds and to reduce the repulsive ionic interactions as much as possible, and giving rise to a massive increase in the cohesive energy and a geometrical phase transition. The minimum A at $a=13.8$ Å is another equilibrium point, which shows that phase A of Mg_3B_{80} emerges, which may be formed by both covalent and ionic bondings. The compression of such a solid is very hard, as the energy curve climbs up quickly as a further decreases. A similar analysis applies for K_3B_{80}, whose geometrical phase transition should also come from the competition of covalent and ionic bondings. As mentioned above, while phase B of K_3B_{80} and Mg_3B_{80} are rather similar, phase A of K_3B_{80} and Mg_3B_{80} are rather different in cohesive energies and the formation of intercluster covalent bonds, which may be caused by the disparity in sizes of K and Mg ions. For the fcc K_3C_{60} solid, the tetrahedral interstitial sites can hold less space than octahedral sites,[18] and for the fcc B_{80}, due to the geometrical distortion, the space at tetrahedral site is larger than octahedral site, as they can accommodate spheres of radius 1.6 and 1.26 Å,[27] respectively. Note that the radius of K ion is about 1.38 Å, while the radius of Mg ion is about 0.72 Å,[28] implying that the K ion is too large and hard to be accommodated in the space at the octahedral site, while Mg is perfect. Therefore, for the intercalation of Mg atoms it is not needed to greatly affect the lattice structure of the fcc B_{80}, where phase A of Mg_3B_{80} bears a nearly identical structure to fcc B_{80} and the same number of intercluster covalent bonds are formed. On the other hand, in the formation of phase A of K_3B_{80}, to insert K atoms into the octahedral sites, the intercluster distance should be increased and two of the intercluster covalent bonds have to be broken. In this way, it is easy to understand that the lattice parameters of both phase A and phase B of K_3B_{80} are larger than those of Mg_3B_{80}. As a comparison, we notice that the fcc K_3C_{60} has only one stable phase and no intercluster covalent bonds are formed.

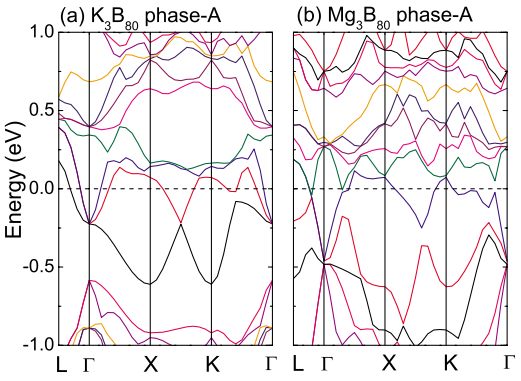

FIG. 4. (Color online) Energy bands of phase A fcc K_3B_{80} and Mg_3B_{80}. The Fermi level is set to zero and indicated by the horizontal dashed line.

This feature may be closely related to the different bonding manners of boron and carbon.

The energy bands and the density of states (DOS) for phase A of fcc K_3B_{80} and Mg_3B_{80} solids are calculated, as presented in Figs. 4 and 5. For K_3B_{80}, the energy bands are quite dispersive and several bands spread across the Fermi level showing that phase A of fcc K_3B_{80} solid is a metal. Note that a gaplike region is located at around 0.5 eV below Fermi energy. Interestingly, the energy bands of phase A of fcc K_3B_{80} exhibit some similar characters to those of the fcc B_{80},[10] especially at Γ point, where there are several corresponding bands with almost the same profiles. Furthermore, both of them have gaplike regions near the Fermi level, while the gaplike region of phase A of the fcc K_3B_{80} is located distinctly under the Fermi level, that of fcc B_{80} is located slightly above the Fermi level. Consistent results could be drawn from the curves of DOS. For phase A of the fcc K_3B_{80}, the DOS has a minimum at about 0.5–0.75 eV under the Fermi energy, while the minimum of DOS for the

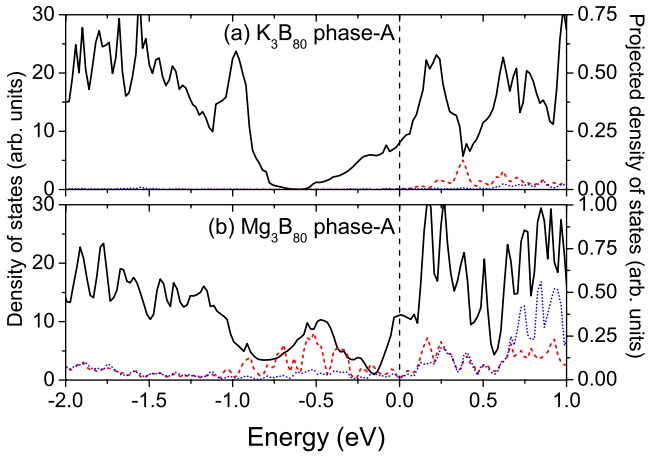

FIG. 5. (Color online) DOS and PDOS of electrons of the fcc K_3B_{80} (a) and Mg_3B_{80} (b), which is obtained by means of the tetrahedra method. The solid (black) line is for DOS, while the dashed (red) line and dotted (blue) line represent PDOS of K_1/Mg_1 and K_2/Mg_2 atoms, respectively. Note that the scales of the vertical axes are different for DOS and PDOS. The Fermi level is set to zero and indicated by the vertical dashed line.

fcc B_{80} stayed slightly above the Fermi level. From another point of view, the K doping does not change the band structure very much, but the Fermi level is shifted up about 0.75 eV. The projected DOS (PDOS) of K atoms vanishes under the Fermi level and only has a peak at about 0.4 eV above the Fermi level, which can be attributed to the 4*s* states of K atoms, revealing that the valence electrons of K atoms are transferred to fill the unoccupied bands derived from the B_{80} unit, lifting the Fermi level up. Apart from the charge population analysis, there is other evidence to confirm the inference that K atoms donate valence electrons to other parts.

The phase *A* of Mg_3B_{80} also has a metallic electronic structure. Several extra bands fill in the gaplike region at 0.5–0.75 eV under the Fermi energy, and in the same energy range, a primary peak (with small peaks) of DOS appears to substitute the minimum of DOS. It is clear that the PDOS of Mg contributes dramatically to this peak. These are the major differences in electronic structures between phase *A* of K_3B_{80} and Mg_3B_{80}. At 0.2–0.4 eV above the Fermi energy, there is also a peak of PDOS derived from Mg indicating the charge transfers from the metallic atoms to boron atoms. Besides, the phase *A* of K_3B_{80} and Mg_3B_{80} have the comparable DOS at the Fermi level, which are mainly caused by the boron atoms. The phase *B* of K_3B_{80} and Mg_3B_{80} are also found to exhibit metallic electronic structures.

V. CONCLUSIONS

In summary, in terms of the first-principles DFT calculations, we predict the possible existence of the stable fcc K_3B_{80} and Mg_3B_{80} solids. It is uncovered that both have two phases (phase *A* and phase *B*) with different lattice parameters. In phase *A*, the B_{80} units are significantly distorted and the intercluster covalent bonds are formed; while in phase *B*, the B_{80} units are slightly distorted and no covalent bonds exist between the neighboring B_{80} units. The phase *A* of Mg_3B_{80} is found to be the most stable phase among them. The different ionic radii and the number of valence electrons of K and Mg atoms give rise to the major geometrical and electronic differences between the fcc K_3B_{80} and Mg_3B_{80} solids. The charge population analysis shows that K and Mg atoms in these solids are ionized and donate electrons to the other boron atoms. The competition of the covalent and ionic bondings may explain the emergence of the two different geometrical phases. The electronic structural calculations reveal that both fcc K_3B_{80} and Mg_3B_{80} solids are metals. It is interesting to note that above the Fermi level, the DOS profile of the fcc Mg_3B_{80} has a small dip that is quite similar to the case of the fcc K_3C_{60} (Ref. 18) implying that the fcc Mg_3B_{80} might also be potentially a superconductor. Our study may stimulate further experimental efforts to obtain these metal-intercalated boron solid phases.

ACKNOWLEDGMENTS

The authors are grateful to X. Chen, S. S. Gong, X. L. Sheng, Z. C. Wang, and L. Z. Zhang for helpful discussions. All of the calculations were completed on the supercomputer NOVASCALE 6800 in the Computer NetWork Information Center (Supercomputing Center) of the Chinese Academy of Sciences. This work was supported in part by the National Science Fund for Distinguished Young Scholars of China (Grant No. 10625419), the MOST of China (Grant No. 2006CB601102), and the Chinese Academy of Sciences.

*Author to whom correspondence should be addressed. gsu@gucas.ac.cn

[1] H. W. Kroto, J. R. Heath, S. C. O'Brien, R. F. Curl, and R. E. Smalley, Nature (London) **318**, 162 (1985).
[2] *Fullerene: Chemistry, Physics and Technology*, edited by K. M. Kadish and R. S. Ruoff (Wiley, New York, 2002).
[3] P. J. Durrant and B. Durrant, *Introduction to Advanced Inorganic Chemistry* (Wiley, New York, 1962).
[4] K. C. Buschbeck, *Boron Compounds, Elemental Boron and Boron Carbides. Gmelin Handbook of Inorganic Chemistry* (Springer, Berlin, 1981), Vol. viii.
[5] E. D. Jemmis and E. G. Jayasree, Acc. Chem. Res. **36**, 816 (2003).
[6] N. Gonzalez Szwacki, A. Sadrzadeh, and B. I. Yakobson, Phys. Rev. Lett. **98**, 166804 (2007).
[7] P. A. Heiney, J. E. Fischer, A. R. McGhie, W. J. Romanow, A. M. Denenstein, J. P. McCauley, A. B. Smith, and D. E. Cox, Phys. Rev. Lett. **66**, 2911 (1991); J. E. Fischer, P. A. Heiney, A. R. McGhie, W. J. Romanow, A. M. Denenstein, J. P. McCauley, and A. B. Smith, Science **252**, 1288 (1991); G. Van Tendeloo, S. Amelinckx, M. A. Verheijen, P. H. M. van Loosdrecht, and G. Meijer, Phys. Rev. Lett. **69**, 1065 (1992).
[8] W. Krätschmer, L. D. Lamb, K. Fostiropoulos, and D. R. Hoffman, Nature (London) **347**, 354 (1990).
[9] A. F. Hebard, M. J. Rosseinsky, R. C. Haddon, D. W. Murphy, S. H. Glarum, T. T. M. Palstra, A. P. Ramirez, and A. R. Kortan, Nature (London) **350**, 600 (1991); K. Holczer, O. Klein, S.-M. Huang, R. B. Kaner, K.-J. Fu, R. L. Whetten, and F. Diederich, Science **252**, 1154 (1991); M. J. Rosseinsky, A. P. Ramirez, S. H. Glarum, D. W. Murphy, R. C. Haddon, A. F. Hebard, T. T. M. Palstra, A. R. Kortan, S. M. Zahurak, and A. V. Makhija, Phys. Rev. Lett. **66**, 2830 (1991).
[10] Q.-B. Yan, Q.-R. Zheng, and G. Su, Phys. Rev. B **77**, 224106 (2008).
[11] R. W. Lof, M. A. van Veenendaal, B. Koopmans, H. T. Jonkman, and G. A. Sawatzky, Phys. Rev. Lett. **68**, 3924 (1992); E. L. Shirley and S. G. Louie, *ibid.* **71**, 133 (1993).
[12] A. Y. Liu, R. R. Zope, and M. R. Pederson, Phys. Rev. B **78**, 155422 (2008).
[13] P. Hohenberg and W. Kohn, Phys. Rev. **136**, B864 (1964).
[14] P. Giannozzi *et al.*, arXiv:0906.2569, http://www.quantum-espresso.org.
[15] D. R. Hamann, M. Schluter, and C. Chiang, Phys. Rev. Lett. **43**, 1494 (1979).
[16] J. P. Perdew and A. Zunger, Phys. Rev. B **23**, 5048 (1981).
[17] W. Kohn and L. J. Sham, Phys. Rev. **140**, A1133 (1965).

[18] S. Saito and A. Oshiyama, Phys. Rev. B **44**, 11536 (1991).
[19] P. W. Stephens, L. Mihaly, P. L. Lee, R. L. Whetten, S.-M. Huang, R. Kaner, F. Deiderich, and K. Holczer, Nature (London) **351**, 632 (1991).
[20] To check the effect of orientational disorder, we have tested other orientations of B_{80} units with lower symmetries as starting configurations. The results suggest that the presumed orientation is energetically more favorable.
[21] J. D. Head and M. C. Zerner, Chem. Phys. Lett. **122**, 264 (1985).
[22] Using the geometrical optimization scheme in this paper, it is also found that B_{80} could also form the phase *A* and phase *B* of fcc B_{80} solids similar to the situation of fcc K_3B_{80} solids. Due to using a different approach to obtain the optimized geometries, our previous work (Ref. 10) found only one stable fcc B_{80} solid phase, which is in fact the phase *A* and is the most stable fcc B_{80} solid phase.
[23] G. Gopakumar, M. T. Nguyen, and A. Ceulemans, Chem. Phys. Lett. **450**, 175 (2008); A. Ceulemans, J. T. Muya, G. Gopakumar, and M. T. Nguyen, *ibid.* **461**, 226 (2008).
[24] Q.-B. Yan, X.-L. Sheng, Q.-R. Zheng, L.-Z. Zhang, and G. Su, Phys. Rev. B **78**, 201401(R) (2008).
[25] 017X.-L. Sheng, Q.-B. Yan, Q.-R. Zheng, and G. Su, Phys. Chem. Chem. Phys. (to be published).
[26] S.-P. Gao, C. J. Pickard, M. C. Payne, J. Zhu, and J. Yuan, Phys. Rev. B **77**, 115122 (2008).
[27] In the fcc B_{80} solid, boron atoms compose small closed cages with radii of 2.45 and 2.11 Å at the tetrahedral and octahedral interstitial sites. These cages can accommodate spheres of radius about 1.6 and 1.26 Å, respectively, if we take into account the radius of the boron atom to be 0.85 Å.
[28] R. D. Shannon, Acta Crystallogr. A **32**, 751 (1976).